Three-dimensional flows over backward facing steps

C. Nonino, G. Comini and G. Croce
Università degli Studi di Udine, Dipartimento di Energetica e Macchine, Udine, Italy

Keywords *Backward facing steps, Finite elements, Three-dimensional flow*

Abstract *Three-dimensional flows over backward facing steps are analysed by means of a finite element procedure, which shares many features with the SIMPLER method. In fact, given an initial or guessed velocity field, the pseudovelocities, i.e. the velocities that would prevail in the absence of the pressure field, are found first. Then, by enforcing continuity on the pseudovelocity field, the tentative pressure is estimated, and the momentum equations are solved in sequence for velocity components. Afterwards, continuity is enforced again to find corrections that are used to modify the velocity field and the estimated pressure field. Finally, whenever necessary, the energy equation is solved before moving to the next step.*

Introduction

In the solution of three-dimensional incompressible flow problems, sequential (or decoupled) methods have a clear advantage over fully coupled methods, especially as the number of nodes increases. As a consequence, a lot of ongoing finite element research is directed towards sequential procedures that have many features in common with well known finite difference algorithms such as the SIMPLE and the SIMPLER methods (Haroutunian *et al.*, 1993; Comini *et al.*, 1996; Patankar and Spalding, 1972; Patankar, 1980).

Among the uncoupled finite element methods, projection algorithms are considered to be quite reliable (Gresho, 1990; Gresho and Chan, 1990). In most projection algorithms the discretized continuity and momentum equations are manipulated to obtain a discretized analogue of the Poisson equation for pressure. In such a case, to avoid overconstraining the velocity field, the functions weighting the continuity equation, i.e. the pressure interpolating polynomials, are chosen to be one degree less than the polynomials interpolating velocity components.

As an alternative, equal order projection algorithms can be derived by obtaining a Poisson equation for pressure from approximations of continuous, rather than discretized, mass and momentum balances. Equal order implementations have the very desirable feature of allowing the same interpolating functions to be used for velocity components and pressure. Furthermore, they yield a true Laplacian matrix in the discretized versions of the pressure equations. This reduces the computing time and, simultaneously improves accuracy when the elements are distorted (Gresho *et al.*, 1995). Most equal order algorithms share some essential features of the SIMPLE procedure since they update the pressure field on the basis of a pressure correction equation related to the velocity corrections necessary to ensure continuity

International Journal of Numerical Methods for Heat & Fluid Flow, Vol. 9 No. 3, 1999, pp. 224-239.

(Patankar and Spalding, 1972). On the other hand, the SIMPLE method is known to yield rather poor pressure corrections, in particular with high Reynolds number flows (Patankar, 1980). Since the same feature is shared by the finite element versions of the scheme, we felt that there was room for the introduction of a SIMPLER-like projection algorithm in the finite element context. In our algorithm, the tentative pressure field is estimated at each time step from a pressure Poisson equation enforcing continuity on the pseudovelocities, i.e. the velocities that would prevail in the absence of the pressure field. Then, the momentum equations are solved in sequence for velocity components, and continuity is enforced again to find corrections that modify both the velocity field and the estimated pressure field. Finally, if required, the energy equation is solved before moving to the next step.

A finite element procedure based on the algorithm outlined above has already been validated in Nonino and Croce (1997) by successfully comparing computed results with literature data referring to typical benchmark problems. In this paper we illustrate detailed computational experiments conducted with reference to isothermal and stratified flow over backward-facing steps. In the isothermal case numerical results are shown to be in very good agreement with the experimental results, of Armaly *et al.* (1982). Isothermal flow over a backward-facing step has already been studied by one of the authors in Nonino (1998). However, due to a geometry different from that of Armaly *et al.* (1982), a complete validation against experimental data was not carried out in that paper. In the stratified flow case there are no comparison data available in the external literature for the three-dimensional problem. In fact, to the authors' knowledge, the only available examples of application have been presented by Nonino *et al.* (1997). Consequently, the illustration of the main features of stratified flows presented here is based on the above mentioned computational experiments.

Statement of the problem

With reference to the Boussinesq approximation, the momentum and continuity equations which govern the laminar flow of a constant property fluid in a three-dimensional domain can be written as

$$\rho \frac{\partial \mathbf{v}}{\partial \vartheta} + \rho \mathbf{v} \cdot \nabla \mathbf{v} = \mu \nabla^2 \mathbf{v} - \nabla p - \rho \beta (t - t_0) \mathbf{g} \tag{1}$$

$$\nabla \cdot \mathbf{v} = 0 \tag{2}$$

respectively. In the above equations, $\mathbf{v}$ is the velocity vector, ϑ is time, ρ is density, μ is the dynamic viscosity, β is the coefficient of thermal expansion, $\mathbf{g}$ is the gravity vector, t is the temperature and p is the pressure evaluated with reference to the hydrostatic conditions at the reference temperature t_0. In the absence of volumetric heating and neglecting the effects of viscous dissipation, the energy equation can be written as

$$\rho c \frac{\partial t}{\partial \vartheta} + \rho c \mathbf{v} \cdot \nabla t = k \nabla^2 t \tag{3}$$

where c is the specific heat and k is the thermal conductivity.

A velocity field must be specified as the initial condition, while appropriate boundary conditions must be imposed on inflow boundaries, outflow boundaries and solid boundaries. At inflow and solid boundaries, we can specify, for example, both velocity

$$\mathbf{v} = \mathbf{v}_p \tag{4}$$

and temperature

$$t = t_p \tag{5}$$

as boundary conditions of the first kind.

At outflow boundaries, in general, we have a fully-developed flow situation which leads to boundary conditions of the second kind, for both velocity

$$\nabla \mathbf{v} \cdot \mathbf{n} = 0 \tag{6}$$

and temperature

$$\nabla t \cdot \mathbf{n} = 0 \tag{7}$$

In equations (6) and (7), $\mathbf{n}$ is the outward normal to the boundary surface. The above assumptions do not reduce the generality of the formulation since different boundary conditions, such as those on symmetry and adiabatic boundaries, can be expressed by combining equations (4) to (7).

Solution procedure

The solution steps are derived in a continuous setting, where no reference is made to the particular space discretization that will be employed afterwards. As we have already pointed out, the tentative pressure p^* is first estimated at each new time step $(n+1)$ on the basis of the velocity field $\mathbf{v}^n$ at the time step n. The pressure estimation is obtained by writing

$$\rho \frac{\hat{\mathbf{v}} - \mathbf{v}^n}{(\Delta \vartheta)_p} + \rho \mathbf{v}^n \cdot \nabla \mathbf{v}^n = \frac{1}{2} \mu \left(\nabla^2 \hat{\mathbf{v}} + \nabla^2 \mathbf{v}^n \right) - \rho \beta (t^n - t_0) \mathbf{g} \tag{8}$$

$$\rho \frac{\mathbf{v}^{n+1} - \hat{\mathbf{v}}}{(\Delta \vartheta)_p} = - \nabla p^* \tag{9}$$

where $\hat{\mathbf{v}}$ is the pseudovelocity, i.e. the velocity that would prevail in the absence of the pressure field, and $(\Delta \vartheta)_p$ is the time step utilised for the purpose of estimating pressure. In equation (8), the advective term is dealt with explicitly, while the diffusion term is approximated by means of a Crank-Nicolson scheme

(Gresho, 1990; Gresho and Chan, 1990). Taking the divergence of equation (9) and assuming

$$\nabla \cdot \mathbf{v}^{n+1} = 0 \tag{10}$$

as a means of enforcing continuity through the action of ∇p^*, we obtain

$$\nabla^2 p^* = \frac{\rho}{(\Delta \vartheta)_p} \nabla \cdot \hat{\mathbf{v}} \tag{11}$$

i.e. the pressure Poisson equation for p^*.

The estimated pressure p^* is utilised to solve the momentum equations by means of the fully implicit scheme

$$\rho \frac{\mathbf{v}^* - \mathbf{v}^n}{(\Delta \vartheta)_v} + \rho \mathbf{v}^n \cdot \nabla \mathbf{v}^* = \mu \nabla^2 \mathbf{v}^* - \nabla p^* - \rho \beta (t^n - t_0) \mathbf{g} \tag{12}$$

where $\mathbf{v}^*$ is the velocity field that corresponds to p^*, and the time step $(\Delta \vartheta)_v$ is usually larger than $(\Delta \vartheta)_p$. Since $\mathbf{v}^*$, in general, does not respect continuity, we can find pressure corrections p' which "project" $\mathbf{v}^*$ onto the divergence-free space $\mathbf{v}^{n+1}$ by writing

$$\rho \frac{\mathbf{v}^{n+1} - \mathbf{v}^*}{(\Delta \vartheta)_v} = \rho \frac{\mathbf{v}'}{(\Delta \vartheta)_v} = -\nabla p' \tag{13}$$

where $\mathbf{v}'$ is the velocity correction field. Taking the divergence of equation (13) and assuming the validity of equation (10) as a means of enforcing continuity through the action of $\nabla p'$, we obtain

$$\nabla^2 p' = \frac{\rho}{(\Delta \vartheta)_v} \nabla \cdot \mathbf{v}^* \tag{14}$$

i.e. the pressure Poisson equation for p'. Finally, we use p' to compute the pressure field

$$p^{n+1} = p^* + p' \tag{15}$$

and $\mathbf{v}'$, obtained from equation (13), to compute the velocity field

$$\mathbf{v}^{n+1} = \mathbf{v}^* + \mathbf{v}' \tag{16}$$

One may wonder why the pressure correction step (15) is utilised here, while it is not considered in the SIMPLER algorithm. The reason is that the pressure equation (11) has been derived from differential forms of the momentum and continuity equations. As a consequence, when equation (11) is discretized with respect to the space variables, it is not easy to ensure that its terms are consistent with the corresponding pressure terms in the space-discretized version of equation (12). Therefore, p^* must be regarded as an approximate pressure, and the correction (15) really improves the estimate of p at the end of

the time step. Furthermore, by maintaining the pressure correction feature (15), equations (12-15) yield the same SIMPLE-like algorithm described in Comini and Del Giudice (1982). Thus, we can switch the pressure estimation procedure described by equations (8-11) on and off, employing this additional feature only when it is needed, i.e. with high Reynolds number flows.

When the velocity and pressure fields have been computed we can solve, if required, the energy equation before moving to the next step. This equation is discretized by means of the fully implicit scheme

$$\rho c \frac{t^{n+1} - t^n}{(\Delta \vartheta)_t} + \rho c \, \mathbf{v}^n \cdot \nabla t^{n+1} = k \nabla^2 t^{n+1} \tag{17}$$

where we assume $(\Delta\vartheta)_t = (\Delta\vartheta)_v$.

Weak forms of the governing equations

The momentum equations (8) and (12), written in Cartesian coordinates, and the energy equation (17) can be considered particular cases of the time-discretized general transport equation (Comini *et al.*, 1994). In the present case, the application of the Bubnov-Galerkin finite element method leads to weak forms where the boundary terms can be disregarded. In fact the nodal equations are not needed where we impose boundary conditions of the first kind, while on the other boundaries we have zero normal-derivative boundary conditions.

The pressure equation (11) and the pressure correction equation (14) are particular forms of the Poisson equation. Following the standard procedure, for each node we obtain a suitable integral form by weighting and integrating the differential equations over the computational domain. Then, the application of Green's theorem to the Laplacians, leads to the weak forms

$$\int_\Omega \nabla W_i \cdot \nabla p^* \, d\Omega + \int_\Omega W_i \frac{\rho}{(\Delta \vartheta)_p} \nabla \cdot \hat{\mathbf{v}} \, d\Omega = \int_S W_i \nabla p^* \cdot \mathbf{n} \, dS = 0 \tag{18}$$

$$\int_\Omega \nabla W_i \cdot \nabla p' \, d\Omega + \int_\Omega W_i \frac{\rho}{(\Delta \vartheta)_v} \nabla \cdot \mathbf{v}^* \, d\Omega = \int_S W_i \nabla p' \cdot \mathbf{n} \, dS = 0 \tag{19}$$

for the pressure equation (11) and the pressure correction equation (14), respectively. By taking into account equations (9) and (13), respectively, the boundary terms in the above equations can be expressed as

$$\int_S W_i \nabla p^* \cdot \mathbf{n} \, dS = \int_S W_i \rho \frac{\mathbf{v}^{n+1} - \hat{\mathbf{v}}}{(\Delta \vartheta)_p} \cdot \mathbf{n} \, dS \tag{20}$$

$$\int_S W_i \nabla p' \cdot \mathbf{n}\, dS = \int_S W_i \rho \frac{\mathbf{v}^{n+1} - \mathbf{v}^*}{(\Delta\vartheta)_v} \cdot \mathbf{n}\, dS \tag{21}$$

The right hand sides of the previous equations are certainly equal to zero on symmetry boundaries or on boundaries where we impose conditions of the first kind ($\mathbf{v}^{n+1} = \hat{\mathbf{v}} = \mathbf{v}^* = \mathbf{v}_p$). Moreover, if, before solving equations (18) and (19), we correct the computed velocity distribution on other boundaries to enforce global mass conservation, we make the right hand sides of equations (20) and (21) equal to zero (Comini *et al.*, 1996). As a consequence, in the solution of the pressure equations, only the pressure levels must be set by the boundary conditions $p^* = 0$ or $p' = 0$ applied on the reference point(s).

Finite element formulation

Substituting the approximations for the nodal values of u, v, w, t, p^*, p and p' into the appropriate weak forms, we arrive at systems of space discretized equations (Comini *et al.*, 1994). The solution strategy outlined in the previous sections leads to the calculation procedure illustrated below.

At the beginning of each time step, we compute the nodal values of the pseudovelocity components from the matrix equations

$$\rho \mathbf{M} \frac{\hat{\mathbf{u}} - \mathbf{u}^n}{(\Delta\vartheta)_p} + \frac{1}{2}\mu \mathbf{K}(\hat{\mathbf{u}} + \mathbf{u}^n) + \rho \mathbf{A}\, \mathbf{u}^n - \rho g_x \beta \mathbf{b} = 0 \tag{22a}$$

$$\rho \mathbf{M} \frac{\hat{v} - v^n}{(\Delta\vartheta)_p} + \frac{1}{2}\mu \mathbf{K}(\hat{v} + v^n) + \rho \mathbf{A}\, v^n - \rho g_y \beta \mathbf{b} = 0 \tag{22b}$$

$$\rho \mathbf{M} \frac{\hat{\mathbf{w}} - \mathbf{w}^n}{(\Delta\vartheta)_p} + \frac{1}{2}\mu \mathbf{K}(\hat{\mathbf{w}} + \mathbf{w}^n) + \rho \mathbf{A}\, \mathbf{w}^n - \rho g_z \beta \mathbf{b} = 0 \tag{22c}$$

based on the weak forms of the Cartesian components of equation (8).

The nodal values of the estimated pressure are computed from the matrix equation

$$\mathbf{K}\, \mathbf{p}^* = -\frac{\rho}{(\Delta\vartheta)_p}(\mathbf{D}^u \hat{\mathbf{u}} + \mathbf{D}^v \hat{v} + \mathbf{D}^w \hat{\mathbf{w}}) \tag{23}$$

based on the weak form (20).

The nodal values of the approximate velocity components are evaluated from the matrix equations

$$\rho \mathbf{M} \frac{\mathbf{u}^* - \mathbf{u}^n}{(\Delta\vartheta)_v} + (\mu \mathbf{K} + \rho \mathbf{A})\, \mathbf{u}^* + \mathbf{D}^u \mathbf{p}^* - \rho g_x \beta \mathbf{b} = 0 \tag{24a}$$

$$\rho \mathbf{M} \frac{v^* - v^n}{(\Delta \vartheta)_v} + (\mu \mathbf{K} + \rho \mathbf{A})\, v^* + \mathbf{D}^v \mathbf{p}^* - \rho g_y \beta \mathbf{b} = 0 \tag{24b}$$

$$\rho \mathbf{M} \frac{\mathbf{w}^* - \mathbf{w}^n}{(\Delta \vartheta)_v} + (\mu \mathbf{K} + \rho \mathbf{A})\, \mathbf{w}^* + \mathbf{D}^w \mathbf{p}^* - \rho g_z \beta \mathbf{b} = 0 \tag{24c}$$

based on the weak forms of the Cartesian components of equation (12).

The nodal values of the correction pressure are computed from the matrix equation

$$\mathbf{K}\, \mathbf{p}' = -\frac{\rho}{(\Delta \vartheta)_v} (\mathbf{D}^u\, \mathbf{u}^* + \mathbf{D}^v\, \mathbf{v}^* + \mathbf{D}^w\, \mathbf{w}^*) \tag{25}$$

based on the weak form (21).

The nodal values of the velocity-correction components are evaluated from the matrix equations

$$\rho \bar{\mathbf{M}} \frac{\mathbf{u}'}{(\Delta \vartheta)_v} = -\mathbf{D}^u \mathbf{p}' \tag{26a}$$

$$\rho \bar{\mathbf{M}} \frac{v'}{(\Delta \vartheta)_v} = -\mathbf{D}^v \mathbf{p}' \tag{26b}$$

$$\rho \bar{\mathbf{M}} \frac{\mathbf{w}'}{(\Delta \vartheta)_v} = -\mathbf{D}^w \mathbf{p}' \tag{26c}$$

which correspond to the Cartesian components of equation (13). In equations (42), $\bar{\mathbf{M}}$ indicates the mass matrix lumped by the usual row-summing technique.

At the end of the time step, the nodal values of velocity components and the pressure are updated, according to the obvious formulae

$$\mathbf{u}^{n+1} = \mathbf{u}^* + \mathbf{u}' \tag{27a}$$

$$v^{n+1} = v^* + v' \tag{27b}$$

$$\mathbf{w}^{n+1} = \mathbf{w}^* + \mathbf{w}' \tag{27c}$$

$$\mathbf{p}^{n+1} = \mathbf{p}^{*} + \mathbf{p}' \tag{28}$$

Finally, the nodal values of temperature t^{n+1} are computed from the matrix equation

$$\rho c\, \mathbf{M} \frac{\mathbf{t}^{n+1} - \mathbf{t}^{n}}{(\Delta \vartheta)_v} + (k\,\mathbf{K} + \rho c\, \mathbf{A})\, \mathbf{t}^{n+1} = 0 \tag{29}$$

based on the weak form of equation (17).

Standard definitions, not reported here for the sake of brevity, apply to matrix and vector entries appearing in the previous equations (Nonino and Comini, 1997).

Numerical results

The reliability of the numerical procedure described in the previous section has already been demonstrated in Nonino and Croce (1997) by comparing computed results with literature data for typical benchmark problems. In this paper the numerical examples concern three-dimensional isothermal and stratified flows over backward-facing steps.

Isothermal flow

Isothermal flow over a backward facing step has been considered first. We call s the step height, h the inlet channel height (total channel height is thus $h_t = s + h$). Step height to inlet channel height ratio is $s/h = 0.9423$ and the channel width is $W = 34.61h$, in order to compare our results to experimental data (Armaly *et al.*, 1982) and numerical results from other authors (Williams and Baker, 1996). For Reynolds numbers below Re = 400 flow should nearly recover 2D results, at least in terms of midspan reattachment length (Armaly *et al.*, 1982); 3D numerical results are available, to authors' knowledge, up to Re = 800. Three values of the Reynolds number have thus been considered, Re = 400, 600, 800, in order to evaluate significant 3D flow configuration and further validate the code.

All model equations have been cast in non-dimensional form, using the double of inlet channel height $H = 2h$, the average inlet velocity U_0 and the time $\Theta = H/U_0$ as reference length, velocity and time, respectively. The dimensionless domains considered are $0 < x < 15$, $-8.65 < y < 8.65$ and $-0.47115 < z < 0.5$. The fully developed velocity profiles at inlet was calculated from the equation (Shah and London, 1978)

$$u = u_{\max} \left[1 - \left(\frac{|z - 0.25|}{0.25}\right)^2\right] \left[1 - \left(\frac{2\ |y|}{W/H}\right)^m\right] \tag{30}$$

with $u_{\max} = 1.501$ $m = 13.6$.

Thus, the specified boundary conditions are:

- u given by equation (30), $v = w = 0$ on the inlet section ($x = 0, 0 < z < 0.5$);
- $u = v = w = 0$ on the step wall ($x = 0, -0.47115 < z < 0$) and on the lateral walls ($y = \pm 8.65$);
- $u = v = w = 0$ and on the top wall ($z = 0.5$);
- $u = v = w = 0$ and on the bottom wall ($z = -0.47115$);
- $\partial u/\partial n = \partial v/\partial n = \partial w/\partial n = 0$ at the outlet ($x = 15$);
- $p = 0$ at a node at $y = 0$ and $z = -0.5$ on the outlet section ($x = 15$), on the symmetry plane.

The initial conditions are $u = 0.5, v = w = 0, p = 0$ in the whole domain.

Symmetry considerations allowed the reduction of the computational domain in the y direction to $0 < y < 8.65$. A grid of 90x30x16 linear elements has been used, with grid points clustered near inlet section in x direction and near solid walls in y and z direction. Time steps $(\Delta \vartheta)_p = 0.025$ and $(\Delta \vartheta)_v = 0.05$ have been chosen.

Velocity vectors and pressure contours on the midspan symmetry plane ($y = 0$), for the case Re = 800, are shown in Figure 1. The flow structure appears similar to the well-known two-dimensional case, with a large primary recirculating region downstream of the step and a secondary one near the top wall.

Three-dimensional effects can be detected from the streamlines plots, presented in Figure 2 for the three different Reynolds number. Vortices at the vertical endwalls are present at all Reynolds numbers. The development of these vortices is described in Figure 3, showing, for the Re = 800 case, velocity vectors near vertical end wall on three cross-section planes at different distances from inlet ($x = 2, 4, 6, 8$). The pressure field on vertical and bottom walls is shown in Figure 4.

In order to identify recirculating regions, computed oil flow streaklines on the bottom and top wall of the channel are shown in Figure 5. High Reynolds numbers stress the importance of 3D effects, and the upper recirculation is reduced with respect to literature results for 2D computation (Williams and Baker, 1996).

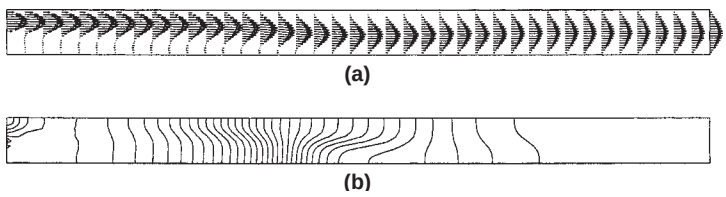

Figure 1.
Isothermal flow: (a) velocity vectors and (b) pressure contour on midspan plane, Re = 800. Pressure values from –0.07 to 0.1743, step 0.0063

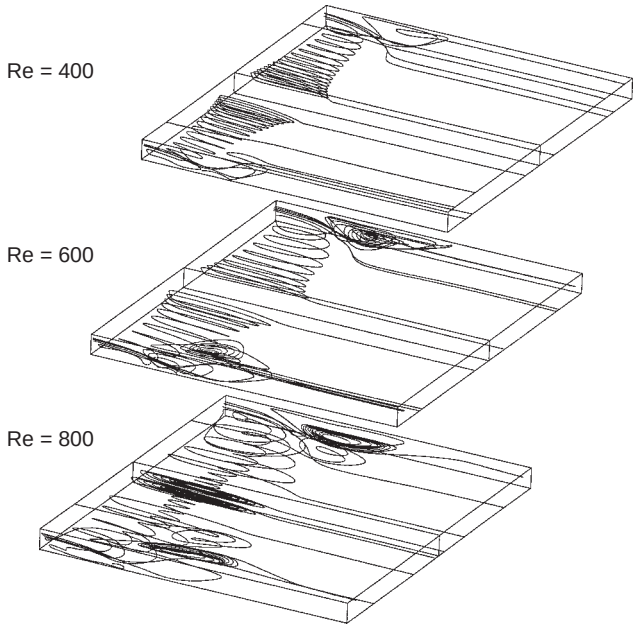

Figure 2.
Isothermal flow: streamlines at Re = 400, 600, 800

Computed values for the reattachment length of the primary vortex at the midspan plane ($y = 0$) are compared in Figure 6 with experimental data and numerical results from other authors. Present results for the three-dimensional flow show very good agreement with experimental data of Armaly *et al.* (1982), and with the 3D computation of Williams and Baker (1996). Two-dimensional prediction from the present method and from other authors (Gartling, 1990;

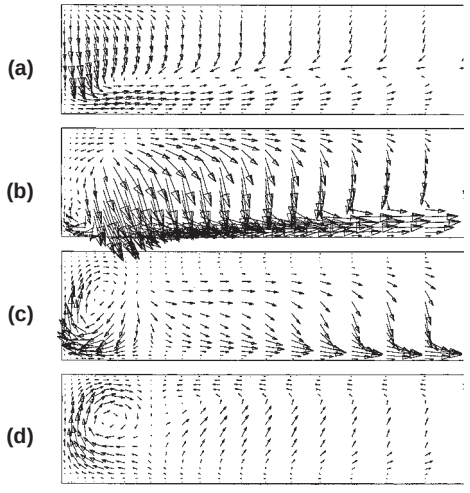

Figure 3.
Isothermal flow: velocity vectors on three cross-section planes at different distances from inlet: (a): x = 2; (b): x =4; (c): x = 6; (d): x = 8; Re = 800

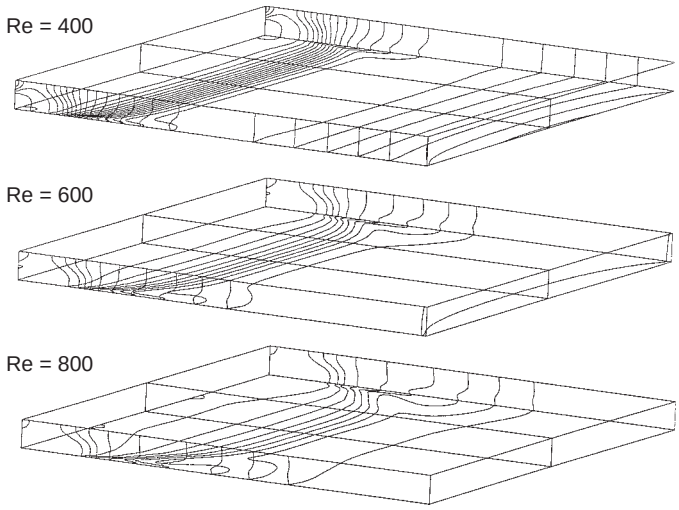

Figure 4.
Isothermal flow: pressure contours on bottom and side walls, Re = 400, 600, 800

Sohn, 1988; Williams and Baker, 1996) are also reported in Figure 5. In order to compare our results with 2D literature data, computations have been carried out with a s/H ratio of 0.5, the same used by Gartling (1990) and Sohn (1988), while Williams and Baker (1996), considered $s/H = 0.47115$. The agreement of the present method with Gartling (1990) reference results is fully satisfying, while all the computations show that 3D effects become significant only for values of the Reynolds number higher than 400.

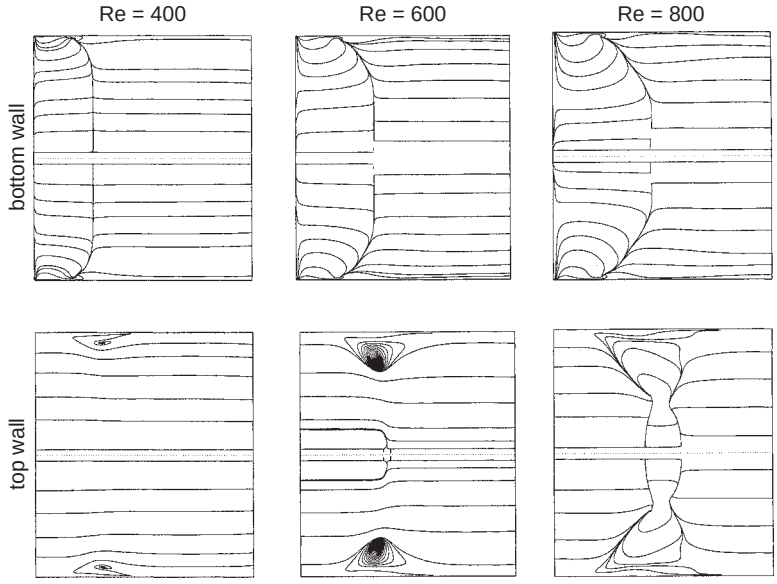

Figure 5.
Isothermal flow: oil flow streaklines on bottom and top wall, Re = 400, 600, 800

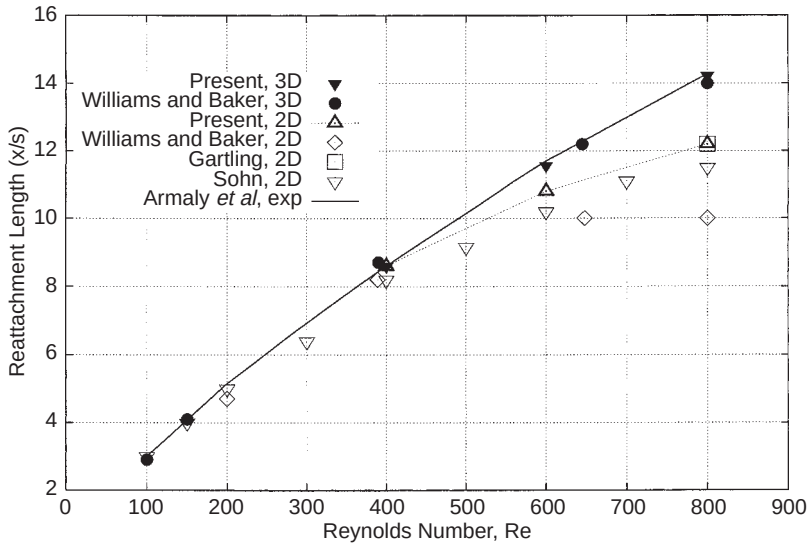

Figure 6.
Isothermal flow: primary reattachment length

Stratified flow

In this section stratified flow with Reynolds number Re = 800, Prandtl number Pr = 1 and Froude number Fr = Re^2/Gr = 16/9 has been considered. A step height equal to 1/2 of the channel height H and two channel widths W, namely $W = 2.5H$ and $W = 5H$, have been considered. This test case has been extensively studied in two-dimensions by Leone (1990), but, at least to the authors' knowledge, there are no comparison data available in the external literature for the corresponding three-dimensional problem, the only exception being the example of application presented by Nonino *et al.* (1997).

All model equations have been cast in non-dimensional form, as in the isothermal flow; the dimensionless temperature is defined as $t = (T - T_c)/(T_h - T_c)$, where T_h and T_c represent the temperatures of the top (hot) and bottom (cold) walls. The dimensionless domains considered are $0 < x < 15$, $-0.5W/H < y < 0.5W/H$ and $-0.5 < z < 0.5$. Boundary conditions for velocity and pressure are the same as in the isothermal flow case, with the fully developed velocity profiles at inlet calculated from the equation (30) with $u_{\max} = 1.73$ and $m = 6.6$ for $W = 2.5H$, and $u_{\max} = 1.61$ and $m = 13.6$ for $W = 5H$. The assumed inlet temperature distribution is given by

$$t = 2\,z \tag{31}$$

Thus, the specified thermal boundary conditions are:

- t given by equation (31) on the inlet section ($x = 0, 0 < z < 0.5$);
- $\partial t/\partial n = 0$ on the step wall ($x = 0, -0.5 < z < 0$) and on the lateral walls ($y = \pm 0.5W/H$);

- $t = 1$ on the top wall ($z = 0.5$);
- $t = 0$ on the bottom wall ($z = -0.5$);
- $\partial t/\partial n = 0$ at the outlet ($x = 15$);

The initial conditions are $u = 0.5$, $v = w = 0$, $p = 0$ and $t = 0.5$ in the whole domain. The assumed value for the reference temperature t_0 is 0.

Symmetry considerations allowed the reduction of the computational domain in the y direction to $0 < y < 0.5W/H$. Regardless of the channel width, the grid employed consists of 90x20x16 linear elements (28,800 elements and 32487 nodes) of equal size in the x and z directions ($\Delta x = 0.166665$ and $\Delta z = 0.0625$) and stretched in the y direction, with the minimum size near the lateral wall and the maximum size near the symmetry plane. The selected values of $(\Delta\vartheta)_p$ and $(\Delta\vartheta)_v = (\Delta\vartheta)_t$ were equal to 0.05 and 0.1, respectively, for both test cases. Calculations were stopped when the Euclidean norms of the velocity change between two successive time steps were less than $1x10^{-6}$. Once again, no upwinding techniques were employed.

With reference to the channel width $W = 5H$, plots of the velocity vectors and of the pressure and temperature contours on the symmetry plane are shown in Figure 7.

The three-dimensional structure of the velocity field and its effects on the pressure distributions are apparent in Figures 8 and 9, showing pressure contours on bottom and vertical walls and oil flow streaklines on horizontal walls.

The wavy flow pattern near the lateral walls, apparent in Figure 8, is due to the presence of recirculation regions on the transverse cross-section of the channel.

Conclusions

A finite element procedure is described for the solution of two- and three-dimensional incompressible laminar flows using primitive variables and equal order interpolations for velocity components, temperature and pressure. The algorithm is cast in a time dependent form which shares many features with the SIMPLER finite difference method.

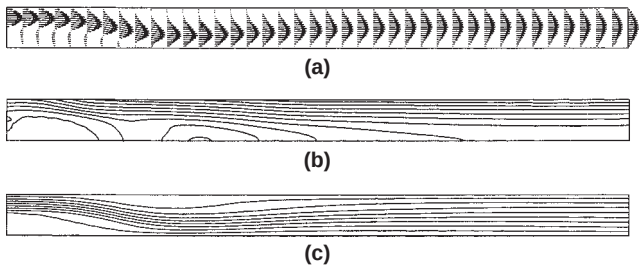

Figure 7.
Test case with W=5H, symmetry plane:
(a) velocity vectors;
(b) pressure contours, values from –0.16 to 0.26, step 0.04;
(c) temperature contours, values from 0.1 to 0.9, step 0.1

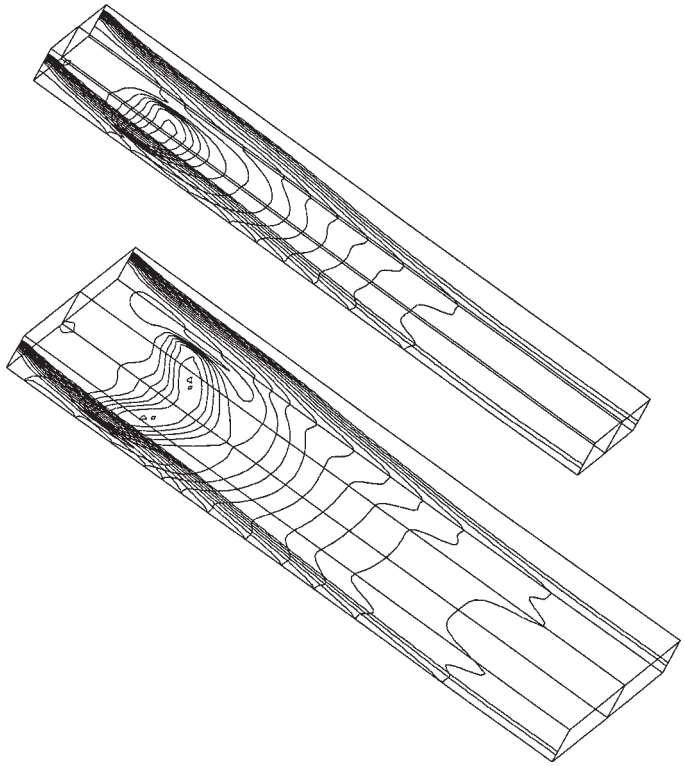

Figure 8.
Stratified flow, pressure contours on bottom and side walls, $W = 2.5H$, $W = 5H$

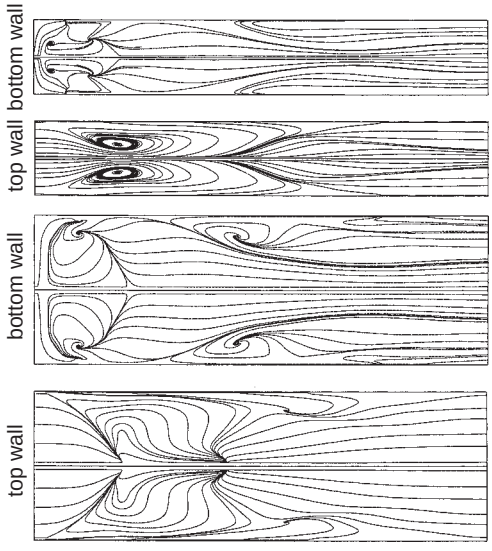

Figure 9.
Test case with $W = 5H$, stratified flow, oil flow streaklines on bottom and top wall, $W = 2.5H$, $W = 5H$

The numerical simulations reported in this paper concern the three-dimensional isothermal and stratified flow over backward-facing steps in channels of different widths. In spite of the use of equal order shape functions in the approximation of both velocity and pressure, the calculated pressure fields never show any sign of checkerboarding.

References

Armaly, B.F., Durst, F., Pereira, J.C.F. and Shonung, B. (1982), "Experimental and theoretical investigation of backward-facing step flow", *J. Fluid Mech.*, Vol. 127, pp. 473-96.

Comini, G. and Del Giudice, S. (1982), "Finite-element solution of the incompressible Navier-Stokes equations", *Numer. Heat Transfer*, Vol. 5, pp. 463-78.

Comini, G., Del Giudice, S. and Nonino, C. (1994), *Finite Element Analysis in Heat Transfer: Basic Formulation and Linear Problems*, Taylor & Francis, Washington, DC.

Comini, G., Minkowycz, W.J. and Shyy, W. (1996), "General algorithms for the finite element solution of incompressible flow problems using primitive variables", in Minkowycz, W.J. and Sparrow, E.M. (Eds), *Advances in Numerical Heat Transfer*, Vol. 1, Taylor & Francis, Washington, DC, pp. 137-70.

Gartling, D.K. (1990), "A test problem for outflow boundary conditions-flow over a backward-facing step", *Int. J. Num. Meth. Fluids*, Vol. 11, pp. 953-67.

Gresho, P.M. (1990), "On the theory of semi-implicit projection methods for viscous incompressible flow and its implementation via a finite element method that also introduces a nearly consistent mass matrix. Part 1: theory", *Int. J. Num. Meth. Fluids*, Vol. 11, pp. 587-620.

Gresho, P.M. and Chan, S.T. (1990), "On the theory of semi-implicit projection methods for viscous incompressible flow and its implementation via a finite element method that also introduces a nearly consistent mass matrix. Part 2: implementation", *Int. J. Num. Meth. Fluids*, Vol. 11, pp. 621-59.

Gresho, P.M., Chan, S.T., Christon, M.A. and Hindmarsh, C. (1995), "A little more on stabilized for transient viscous incompressible flow", *Int. J. Num. Meth. Fluids*, Vol. 21, pp. 837-56.

Haroutunian, V., Engelman, M.S. and Hasbani, I. (1993), "Segregated finite element algorithms for the numerical solution of large-scale incompressible flow problems", *Int. J. Num. Meth. Fluids*, Vol. 17, pp. 323-48.

Leone, J.M. Jr (1990), "Open boundary condition symposium benchmark solution: stratified flow over a backward-facing step", *Int. J. Numer. Methods Fluids*, Vol. 11, pp. 969-84.

Nonino, C. (1998), "Finite element solution of three-dimensional incompressible flows", in Hafez, M. and Heinrich, J.C. (Eds), *Proc. of the 10 Int. Conf. on Finite Elements in Fluids*, Tucson, AZ, pp. 76-91.

Nonino, C. and Comini, G. (1997), "An equal-order velocity-pressure algorithm for incompressible thermal flows. Part 1: formulation", *Numer. Heat Transfer*, Part B, Vol. 32, pp. 1-16.

Nonino, C. and Croce, G. (1997), "An equal-order velocity-pressure algorithm for incompressible thermal flows. Part 2: validation", *Numer. Heat Transfer*, Part B, Vol. 32, pp. 17-35.

Nonino, C., Comini, G. and Croce, G. (1997), "Finite element solution of three-dimensional thermal flows", in Lewis, R.W. and Cross, J.T. (Eds), *Numerical Methods in Thermal Problems*, Vol. 10, Pine Ridge Press, Swansea.

Patankar, S.V. (1980), *Numerical Heat Transfer and Fluid Flow*, Hemisphere, Washington, D.C.

Patankar, S.V. and Spalding, D.B. (1972), "A calculation procedure for heat, mass and momentum transfer in three-dimensional parabolic flows", *Int. J. Heat Mass Transfer*, Vol. 15, pp. 1787-806.

Shah, R.K. and London, A.L. (1978), *Laminar Flow Forced Convection in Ducts*, Academic Press, New York, NY.

Sohn, J.L. (1988), "Evaluation of FIDAP on some classical laminar and turbulent benchmarks", *Int. J. Num. Meth. Fluids*, Vol. 8, pp. 1469-90.

Williams, P.T. and Baker, A.J. (1996), "Incompressible computational fluid dynamics and the continuity constraint method for the three dimensional Navier Stokes equations", *Numer. Heat Transfer*, Part B, Vol. 29, pp. 137-273.